

## Two-dimensional electron gas related emissions in ZnMgO/ZnO heterostructures

Hui Chen, Shulin Gu, Jiagao Liu, Jiandong Ye, Kun Tang et al.

Citation: *Appl. Phys. Lett.* **99**, 211906 (2011); doi: 10.1063/1.3662964

View online: <http://dx.doi.org/10.1063/1.3662964>

View Table of Contents: <http://apl.aip.org/resource/1/APPLAB/v99/i21>

Published by the [American Institute of Physics](http://www.aip.org).

---

### Related Articles

Structural properties of InN films grown on O-face ZnO(000) by plasma-assisted molecular beam epitaxy  
*Appl. Phys. Lett.* **100**, 152105 (2012)

Tunable deformation and electronic properties of single-walled ZnO nanotubes under a transverse electric field  
*J. Appl. Phys.* **111**, 073704 (2012)

Elevated temperature dependence of energy band gap of ZnO thin films grown by e-beam deposition  
*J. Appl. Phys.* **111**, 073511 (2012)

On the origin of an additional Raman mode at 275 cm<sup>-1</sup> in N-doped ZnO thin films  
*J. Appl. Phys.* **111**, 063530 (2012)

CdSe/CdTe type-II superlattices grown on GaSb (001) substrates by molecular beam epitaxy  
*Appl. Phys. Lett.* **100**, 121908 (2012)

---

### Additional information on *Appl. Phys. Lett.*

Journal Homepage: <http://apl.aip.org/>

Journal Information: [http://apl.aip.org/about/about\\_the\\_journal](http://apl.aip.org/about/about_the_journal)

Top downloads: [http://apl.aip.org/features/most\\_downloaded](http://apl.aip.org/features/most_downloaded)

Information for Authors: <http://apl.aip.org/authors>

## ADVERTISEMENT

<p>INSTRUMENTS FOR ADVANCED SCIENCE</p> 	<p><b>Gas Analysis</b></p> <p>dynamic measurement of reaction gas streams catalysis and thermal analysis molecular beam studies dissolved species probes fermentation, environmental and ecological studies</p>	<p><b>Surface Science</b></p> <p>UHV TPD SIMS end point detection in ion beam etch elemental imaging - surface mapping</p>	<p><b>Plasma Diagnostics</b></p> <p>plasma source characterisation etch and deposition process reaction kinetic studies analysis of neutral and radical species</p>	<p><b>Vacuum Analysis</b></p> <p>partial pressure measurement and control of process gases reactive sputter process control vacuum diagnostics vacuum coating process monitoring</p>
	<p>contact Hiden Analytical for further details: <a href="mailto:info@hiden.co.uk">info@hiden.co.uk</a> <a href="http://www.HidenAnalytical.com">www.HidenAnalytical.com</a> <a href="#">CLICK TO VIEW OUR PRODUCT CATALOGUE</a></p>			

## Two-dimensional electron gas related emissions in ZnMgO/ZnO heterostructures

Hui Chen,<sup>1</sup> Shulin Gu,<sup>1,a)</sup> Jiagao Liu,<sup>1</sup> Jiandong Ye,<sup>2</sup> Kun Tang,<sup>1</sup> Shunming Zhu,<sup>1</sup> and Youdou Zheng<sup>1</sup>

<sup>1</sup>*School of Electronic Science and Engineering and Nanjing National Laboratory of Microstructures, Nanjing University, Nanjing 210093, China*

<sup>2</sup>*Department of Electronic Materials Engineering, Research School of Physics and Engineering, The Australia National University, Canberra 0200, Australia*

(Received 28 April 2011; accepted 1 November 2011; published online 22 November 2011)

Radiative recombination of two-dimensional electron gas (2DEG), induced by polarization and validated by Hall effect measurements, is investigated in ZnMgO/ZnO heterostructures grown by metal-organic chemical vapor deposition. The Mg composition, the depth profile distribution of Mg, the residual strain in ZnMgO caplayer, and the thickness of caplayer all significantly influence the 2DEG-related transitions in ZnMgO/ZnO heterostructures. Below or above ZnO donor bound exciton, three additional broad emissions persisting up to 100 K are assigned to the spatially indirect transitions from 2DEG electrons to the photoexcited holes towards the ZnO flat-band region or remaining at the heterointerface. © 2011 American Institute of Physics. [doi:10.1063/1.3662964]

In polar ZnMgO/ZnO heterostructures, polarization engineering will form high-mobility 2DEGs, a topic that has been attracting much attention recently.<sup>1,2</sup> So far, several reports have shown that 2DEGs can be realized in ZnMgO/ZnO heterostructures grown by molecular-beam epitaxy (MBE).<sup>1</sup> In contrast, it has been much more difficult to fabricate 2DEGs in ZnMgO/ZnO heterostructures using metal-organic chemical vapor deposition (MOCVD) which is compatible with mass production for device applications, because of degraded material quality and near-thermal-equilibrium growth conditions.<sup>3,4</sup> 2DEGs at the ZnMgO/ZnO interface have been identified by means of electrical measurements,<sup>1,2,5</sup> but reports<sup>6</sup> that focus on the optical properties of ZnMgO/ZnO do not mention 2DEG-related emissions in heterostructures. In theory, it is difficult to detect 2DEG-related emissions, because holes, necessary for radiative recombination, are pushed into the ZnO flat-band region by the polar electric field. Optical emission below the exciton lines in AlGaIn/GaN observed in earlier studies is believed to be the recombination of quasi-two dimensional (quasi-2D) electrons trapped at the heterointerface and holes towards GaN flat-band. Its intensity drastically diminishes with increasing temperature and the activation energy is less than 10 meV,<sup>7</sup> very low compared with exciton binding energy.

We report here on our recent results using MOCVD growth of ZnMgO/ZnO heterostructures. Temperature-dependent Hall effect measurements reveal that 2DEG has formed in these ZnMgO/ZnO heterostructures. Furthermore, 2DEG-related optical transitions in low-temperature photoluminescence spectra are observed. Photoluminescence in ZnMgO/ZnO heterostructures is strongly influenced by the Mg composition, the distribution profile, and the thickness of the ZnMgO caplayer.

Zn<sub>1-x</sub>Mg<sub>x</sub>O/ZnO heterostructures were grown on sapphire (0001) substrates using metal-organic chemical vapor deposition. First, a high-quality ZnO template was grown in

a MOCVD system (Aixtron) in a close-coupled showerhead (CCS) configuration. We note that the deposited ZnO layer exhibits an excellent crystal quality and layer-by-layer surface morphology.

Four samples with different Zn<sub>1-x</sub>Mg<sub>x</sub>O layers, marked as A, B, C, and D, were grown on the above ZnO templates. For samples A and B, undoped Zn<sub>1-x</sub>Mg<sub>x</sub>O layers with thickness of 20 nm and 60 nm were grown at 920 °C in the same reactor by using dimethylzinc (DMZn) and bis-methylcyclopentadienyl magnesium (MeCp<sub>2</sub>Mg) as Zn and Mg sources, respectively. For samples C and D, however, the undoped Zn<sub>1-x</sub>Mg<sub>x</sub>O layer, 170 nm thick, were grown using DEZn and MeCp<sub>2</sub>Mg in another MOCVD reactor, which is operated at a low temperature of 500 °C. Mg compositions determined from the reflection spectra are 0.20, 0.20, 0.28, and 0.33 for samples A, B, C, and D, respectively.

Temperature-dependent Hall effect measurements in the Van der Pauw configuration, using indium (In) as contact electrodes, were performed to examine the electric properties of these samples. Temperature-dependent photoluminescence (PL) spectra were recorded in the temperature range 10-300 K, excited by a He-Cd laser ( $\lambda = 325$  nm) with a spectrum resolution of 0.2 nm. Secondary-ion mass spectrometry (SIMS) was performed to investigate the diffusion of aluminum (Al) from sapphire (Al<sub>2</sub>O<sub>3</sub>) into ZnO template as well as Mg depth profile in the ZnMgO layer.

The temperature-dependent mobility and carrier concentration for ZnO template and Zn<sub>0.8</sub>Mg<sub>0.2</sub>O/ZnO with 20 nm (sample A) or 60 nm (sample B) caplayer are shown in Figs. 1(a) and 1(b), respectively. In Fig. 1(a), the mobility of ZnO template is about 10 cm<sup>2</sup>/Vs at 10 K, whereas the mobilities of the ZnMgO/ZnO sample with 20-nm-thick and 60-nm-thick caplayers reach the value of 1879 cm<sup>2</sup>/Vs and 1516 cm<sup>2</sup>/Vs, respectively. The obvious increase of the mobility from ZnO template to ZnMgO/ZnO indicates the 2DEG forming at the interface of the heterostructures. The dramatically increased mobility with decreasing temperature is also significant evidence of a 2DEG.<sup>5</sup> As Fig. 1(b) shows, the carrier

<sup>a)</sup>Electronic mail: slgu@nju.edu.cn.

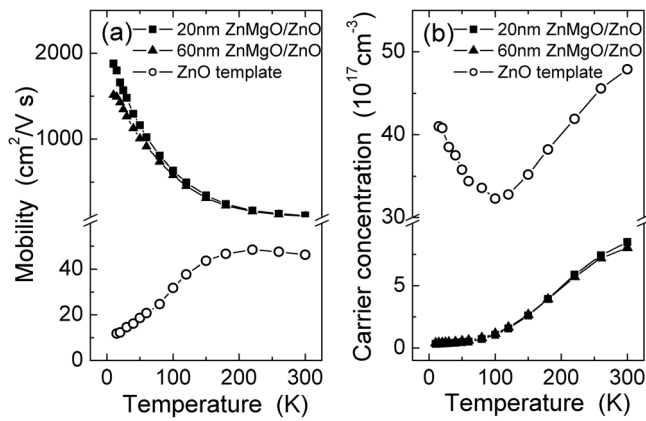


FIG. 1. Temperature-dependent (a) mobility and (b) carrier concentration of ZnO template, samples A and B.

concentration in the ZnO template initially decreases with decreasing temperature, but at temperatures below 100 K, it increases with a further decrease in temperature. Prior work<sup>1</sup> suggests that this feature can be explained by a degenerate layer at the ZnO/sapphire interface that makes an important contribution to the carrier concentration,<sup>8</sup> especially at low temperatures, where donors in the bulk freeze out. Because Al in sapphire substrate diffused into the ZnO buffer at high growth temperature and acted as a shallow donor in ZnO,<sup>9</sup> we suggest that this parallel conductive layer has caused the measured carrier concentration of A and B to change with temperature.

In order to obtain more information of polar ZnMgO/ZnO heterostructures, low-temperature PL (at 10 K) was employed to investigate their optical properties. As shown in Fig. 2, it is interesting to note that the near-band-edge emission shifts to lower energy when the thickness of caplayer increases. For the ZnO template, strong D<sup>0</sup>X emission can be clearly observed at 3.368 eV, together with its phonon replicas. For sample A, however, besides a weak D<sup>0</sup>X emission, a broad shoulder can be observed at 3.344 eV. For sample B, the intensity of this broad shoulder exceeding D<sup>0</sup>X emission becomes the dominating emission. These phenomena can be well explained by the penetration depth of the excitation laser's light in the samples. In ZnO, the penetration depth of our 325 nm laser is about 61 nm (absorption coefficient  $1.6 \times 10^5 \text{ cm}^{-1}$ ),<sup>10</sup> which implies that the absorption volume of the excitation laser is located near the sample's surface. For ZnO template, strong peak indicated as D<sup>0</sup>X is from the surface of ZnO template absolutely. For sample A with 20 nm ZnMgO caplayer, the laser penetrates through the top 20 nm ZnMgO caplayer, ZnO triangle quantum well (several nm), and into ZnO template. Hence, the broad emission in its PL spectrum includes information of all these layers. And for sample B, however, the laser can hardly penetrate to ZnO template due to the thick ZnMgO caplayer. Its PL emission should come from ZnMgO caplayer (60 nm) and ZnO triangle quantum well but with little contribution from ZnO template. In Fig. 2 from bottom to top, with the thickness of the ZnMgO caplayer increasing, the emission at 3.344 eV increases obviously which indicates that this emission must have certain relationship with ZnMgO or 2DEG at triangle quantum well. Due to its energy position below D<sup>0</sup>X line of ZnO, it is more likely to be assigned as 2DEG-related recombination. Moreover, polarization induced field may lead high

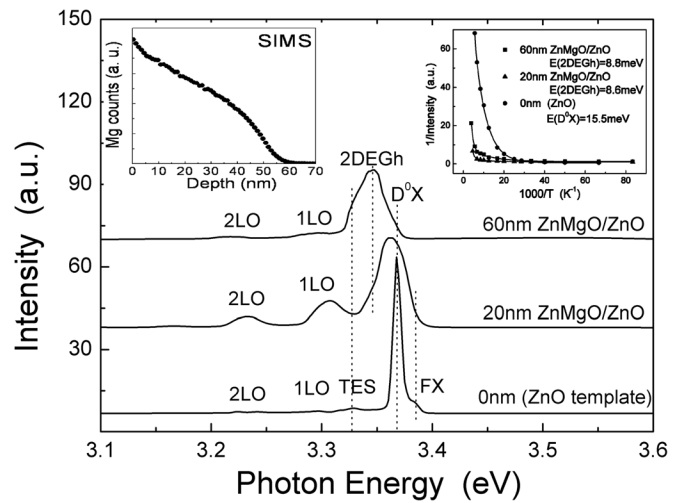


FIG. 2. Low-temperature photoluminescence spectra of ZnO template, samples A and B with different ZnMgO thicknesses. Left inset: SIMS of Mg composition changing with the thickness in B sample. Right inset: Arrhenius plot of the integrated intensity of 2DEG emissions with the temperature according to the equation  $I(T) = I(0)/(1 + \sum_i A_i \exp(-E_i/k_B T))$ .

dissociation of the D<sup>0</sup>X right beneath the interface while the 2DEG-related emission may become remarkable due to its high stability under the field. SIMS result of sample B in the left inset of Fig. 2 shows Mg composition gradually increasing toward the surface called the composition pulling effect during the alloy growth by MOCVD.<sup>3</sup> It indicates that 2DEG in ZnMgO/ZnO heterostructure is a quasi-2D distribution instead of 2D in an ideal abrupt junction.

The right inset of Fig. 2 shows the Arrhenius plots of integrated intensity versus temperature to obtain more information of the 2DEG-related emission. For ZnO template, the activation energy of D<sup>0</sup>X is 15.5 meV related to the delocalization of the bound exciton of ZnO. The activation energy of 2DEG-related emission calculated from the temperature-dependent PL of A and B is 8.6 and 8.8 meV, respectively. The activation energy as small as exciton's affirms our supposition of 2DEG-related emission.<sup>3</sup> Thus, the 2DEG-related emission is a sort of excitonic recombination between electrons located in the triangular potential well and free holes towards ZnO flat valence band region. Similar results have been reported in AlGaIn/GaN samples.<sup>7</sup> Therefore, the forming process of the 2DEG-related emission can be summarized as the photoexcited excitons, excited by the laser, evolve into quasi-2D excitons and subsequently recombine as 2DEG-hole (2DEGh) emission peaks. However, there is no obvious ZnMgO-related emission showed up in PL spectra of ZnMgO/ZnO heterostructures. It might be on account of the thin barrier layers with the less effective confinement of carriers.<sup>3</sup>

Thicker barrier ZnMgO layers (170 nm) with higher Mg composition  $x = 0.28$  (sample C) and  $0.33$  (sample D) have then been employed to investigate the emission behaviors of the heterostructures, which were grown at a low temperature to achieve relatively abrupt interface. The laser penetration depths in the ZnMgO alloys are estimated to be about 200 nm for sample C and 370 nm for D.<sup>11</sup> The penetration depths are both larger than the ZnMgO caplayer; therefore, the surface region of ZnO template can be excited by laser and a sharp emission assigned as D<sup>0</sup>X of ZnO is observed obviously in each spectrum in Fig. 3. The small emission at

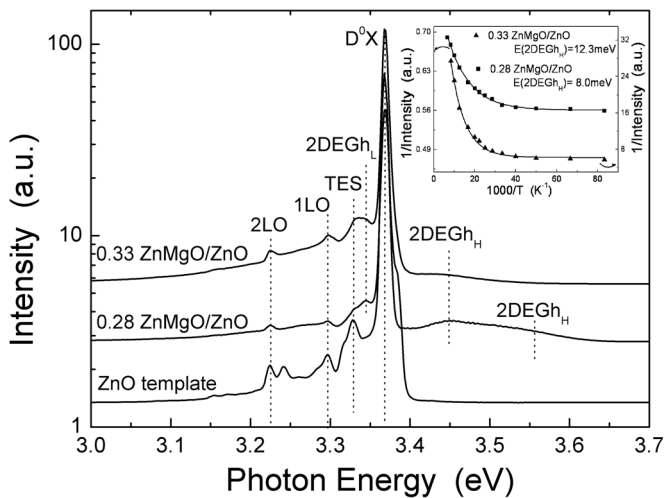


FIG. 3. Low-temperature photoluminescence spectra of ZnO template, samples C and D with different Mg compositions. Inset: Arrhenius plot of the integrated intensity of 2DEG<sub>H</sub> emissions with the temperature according to the equation  $I(T) = I(0)/(1 + \sum_i A_i \exp(-E_i/k_B T))$ .

3.344 eV similar to that observed in samples A and B is assigned as 2DEG<sub>H</sub>. The energy position of 2DEG<sub>H</sub> changes less while D<sup>0</sup>X peak shifts to lower energy position with measuring temperature increased. As a result, a gradual decrease of the energy separation of 2DEG<sub>H</sub> and D<sup>0</sup>X emissions from 24.4 to 21.8 meV is clearly observed when temperature increases from 10 to 60 K, owing to the stronger screening effect of electrons in a triangular potential well at the heterointerface with increasing temperature.<sup>12</sup>

Different from PL spectra of A and B, samples C and D show broad emissions at the higher energy position of D<sup>0</sup>X in Fig. 3. For sample C, the broad emission includes two emissions with different activation energies. The higher energy emission with the activation energy of 31.6 meV might be assigned as the recombination of the 2DEG with the photoexcited holes remaining in the ZnMgO side near the heterointerface (see Fig. 4(b)). For sample D, this emission is not observed due to too high Mg composition in the ZnMgO alloy, where its bandgap energy beyond the laser photons energy and holes cannot be photo-excited. The lower energy emissions, with small activation energies of 8.0 meV for sample C and 12.3 meV for sample D obtained from the inset of Fig. 3, can be assigned to the emissions from 2DEG electrons to holes localized in the heterointerface (2DEG<sub>H</sub>).

Generally, the polarization electric field to form the 2DEG was determined by both spontaneous and piezoelectric polarization effect in the ZnMgO/ZnO heterostructure. According to the previous parameters,<sup>13</sup> we can figure out  $P_{SP(ZnMgO)} - P_{SP(ZnO)} = -0.066x = -0.018 \text{ C/m}^2$ , much smaller than  $P_{PE(ZnMgO)} = 0.095 \text{ C/m}^2$  using  $x = 0.28$ . Therefore, piezoelectric polarization plays a major role in the polarization effect.

To further illustrate the origin of 2DEG emissions of ZnMgO/ZnO heterostructures, the mechanism of 2DEG-related recombination is summarized in the schematic band diagram as shown in Fig. 4. For fully strained ZnMgO/ZnO heterostructure such as samples A and B whose critical thicknesses are both 72 nm (Ref. 14) larger than their real thickness 60 nm, as shown in Fig. 4(a), high piezoelectric

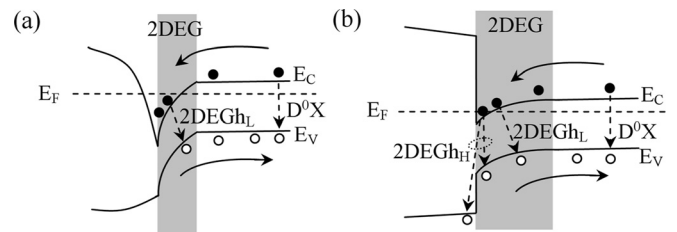


FIG. 4. Schematic band diagram illustration of the ZnMgO/ZnO heterostructures with (a) a narrow 2DEG heterostructure and (b) a wide 2DEG heterostructure. 2DEG<sub>H</sub>L and 2DEG<sub>H</sub>H are the recombinations from the confined 2DEG to free holes towards flat-band of ZnO and interface, respectively.

field may lead a large band bending and form a deep and narrow electron well, with electrons towards the triangular well and holes towards the ZnO flat band region. For partly strained ZnMgO/ZnO heterostructure, such as samples C and D whose critical thicknesses are 48 nm and 39 nm (Ref. 14) smaller than their real thickness (170 nm), low residual strain and small piezoelectric field lead a small band bending and form a shallow and wide electron well resulting in a much smaller Hall mobility ( $\sim 100 \text{ cm}^2/\text{Vs}$ ) of sample D at 10 K (not shown). In the case, a few holes could stay at the heterointerface to recombine with 2DEGs.

In conclusion, we have investigated the radiative recombinations of 2DEGs formed in ZnMgO/ZnO heterostructures grown by MOCVD. Below or above ZnO donor bound excitation, three additional broad emissions are observed and assigned to the spatially indirect transitions from 2DEG electrons to the photoexcited holes towards the ZnO flat-band region or remaining at the heterointerface.

The authors wish to thank Dr. K. L. Teo at IME, Singapore, for providing part of the research samples (ZnO templates, samples A and B). Research is supported by the State Key Program for Basic Research of China under Grant No. 2011CB302003 and National Natural Science Foundation of China (Nos. 61025020 and 60990312).

<sup>1</sup>K. Koike, K. Hama, I. Nakashima, G. Takada, M. Ozaki, K. Ogata, S. Sasa, M. Inoue, and M. Yano, *Jpn. J. Appl. Phys.* **43**, 1372 (2004).

<sup>2</sup>T. Edahiro, N. Fujimura, and T. Ito, *J. Appl. Phys.* **93**, 7673 (2003).

<sup>3</sup>C. B. Soh, S. J. Chua, S. Tripathy, S. Y. Chow, D. Z. Chi, and W. Liu, *J. Appl. Phys.* **98**, 103704 (2005).

<sup>4</sup>J. D. Ye, S. Pannirselvam, S. T. Lim, J. F. Bi, X. W. Sun, G. Q. Lo, and K. L. Teo, *Appl. Phys. Lett.* **97**, 111908 (2010).

<sup>5</sup>K. Koike, K. Hama, I. Nakashima, S. Sasa, M. Inoue, and M. Yano, *Jpn. J. Appl. Phys.* **44**, 3822 (2005).

<sup>6</sup>H. Shibata, H. Tampo, K. Matsubara, A. Yamada, K. Sakurai, S. Ishizuka, S. Niki, and M. Sakai, *Appl. Phys. Lett.* **90**, 124104 (2007).

<sup>7</sup>G. Martínez-Criado, C. Miskys, U. Karrer, O. Ambacher, and M. Stutzmann, *Jpn. J. Appl. Phys.* **43**, 3360 (2004).

<sup>8</sup>K. T. Roro, G. H. Kassier, J. K. Dangbegnon, S. Sivaraya, J. E. Westraadt, J. H. Neethling, A. W. R. Leitch, and J. R. Botha, *Semicond. Sci. Technol.* **23**, 055021 (2008).

<sup>9</sup>K. Tang, S. Gu, S. Li, J. Ye, S. Zhu, H. Chen, J. Liu, R. Zhang, Y. Shi, and Y. Zheng, *J. Vac. Sci. Technol. A* **29**(3), 03A106 (2011).

<sup>10</sup>J. F. Muth, R. M. Kolbas, A. K. Sharma, S. Oktyabrsky, and J. Narayan, *J. Appl. Phys.* **85**, 7884 (1999).

<sup>11</sup>C. W. Teng, J. F. Muth, Ü. Özgür, M. J. Bergmann, H. O. Everitt, A. K. Sharma, C. Jin, and J. Narayan, *Appl. Phys. Lett.* **76**, 979 (2000).

<sup>12</sup>B. Shen, T. Someya, O. Moriwaki, and Y. Arakawa, *Appl. Phys. Lett.* **76**, 679 (2000).

<sup>13</sup>M. Yano, K. Hashimoto, K. Fujimoto, K. Koike, S. Sasa, M. Inoue, Y. Uetsuji, T. Ohnishi, and K. Inaba, *J. Cryst. Growth* **301**, 353 (2007).

<sup>14</sup>H. Matsui, H. Tabata, N. Hasuike, and H. Harima, *J. Appl. Phys.* **99**, 024902 (2006).